Korean J. Chem. Eng., 40(8), 1839-1849 (2023)
DOI: 10.1007/s11814-023-1480-5

pISSN: 0256-1115
eISSN: 1975-7220

Exergy destruction improvement of hydrogen liquefaction process considering variations in cooling water temperature

Dong Hyeon Lee*,‡, Seo Yeon Yu*,‡, Seung Yeol Yeom*, Jeong Jun Lee*, Byeong Chan Kang*, Chung Hun Cho*, Seok Goo Lee,†, and Yeonsoo Kim*,†**

*Department of Chemical Engineering, Kwangwoon University, 20 Kwangwoon-ro, Nowon-gu, Seoul 01897, Korea
**Korea Institute of Industrial Technology, 42-7, Baegyang-daero 804beon-gil, Sasang-gu, Busan 46938, Korea
(*Received 16 February 2023 • Revised 24 April 2023 • Accepted 1 May 2023*)

Abstract−As the movement for carbon neutrality spreads around the world, research on hydrogen energy is also being actively conducted. In the hydrogen value chain, liquefaction is a particularly energy-intensive process. Although the operating energy of the hydrogen liquefaction process can vary greatly depending on the season or regional cooling water temperature, previous studies have not taken this into account. In this study, we quantitatively identify the effect of the change in cooling water temperature on exergy destruction, specific energy consumption (SEC), and coefficient of performance (COP) of the liquefaction process. In addition, we propose a design improvement to reduce exergy destruction with the exergy analysis of multi-stream heat exchangers. A new design (auxiliary process) that reduces exergy destruction is proposed by analyzing the device where energy destruction occurs the most. When the cooling water temperature increases from 20 °C to 35 °C, there is a tendency for SEC and exergy destruction to increase and the COP to decrease. The new design with an auxiliary process shows a decrease in SEC and a reduced rate of increase in SEC in response to the increase in cooling water temperature. The base case without the auxiliary cycle shows that the SEC with cooling water of 35 °C is 14.66% greater than that with cooling water of 20 °C, while the proposed process shows the rate of increase of 9.70%. This means that adding the auxiliary cycle can improve the energy efficiency and increase robustness to variations in ambient conditions.

Keywords: Hydrogen, Liquefaction, Exergy Destruction, Coefficient of Performance, Specific Energy Consumption

INTRODUCTION

The Paris Agreement became international law in 2016 to address the urgent global issue of climate change [1,2]. In 2019, the Climate Action Summit declared the goal of net zero, i.e., zero carbon emissions by 2050. The COP-26 in 2021 further strengthened the nationally determined contribution (NDC) by 2030 to realize carbon neutrality by 2050 [3]. Despite these efforts, Enerdata's 2021 global energy consumption statistics reveal that fossil fuels such as oil and coal still provide 56% of the energy consumed, while only 28.1% of global electricity is generated from renewable sources [4, 5]. To address the global challenge of climate change and promote sustainable development, a change in the energy system is necessary, driven by ongoing research into alternative energy sources. Hydrogen energy has become a focus of interest due to its emission-free combustion and potential to reduce air pollution [6-8].

According to the Korea Trade-Investment Promotion Agency (KOTRA), global hydrogen consumption is expected to reach 1.4 billion tons by 2030 and 660 million tons by 2050, accounting for about 22% of total energy demand. In particular, the potential global market for hydrogen technology is expected to reach $2.5 trillion by 2050 [9]. The EU is establishing a green hydrogen priority strategy through the "Green Deal" in 2019 and the "Hydrogen Strategy" and "Hydrogen IPCEI Agreement" in 2020. The US is pushing for large-scale investment plans related to zero carbon emissions and aggressively investing in hydrogen technology by private companies. Japan is securing price competitiveness by establishing overseas hydrogen supply chains with Australia and Brunei. Australia is trying to reduce hydrogen production costs and solidify its position as a top hydrogen exporter by constructing hydrogen hubs [10,11].

This rapidly expanding hydrogen market has propelled ongoing research on hydrogen production, transportation, storage, and refueling [12]. Liquefaction can drastically reduce the volume and enhance the energy density to facilitate hydrogen storage and transportation [13-15]. However, liquefaction efficiency is somewhat low and the operation cost is high. To commercialize the large-scale hydrogen liquefaction process, it is necessary to reduce the unit operation cost by improving efficiency [16,17].

In 1895, Carl von Linde and William Hampson invented the first liquefaction cycle (the Linde-Hampson cycle) [18]. The Claude cycle, developed by George Claude in 1902, allows liquefaction at a lower temperature than Linde's isenthalpic expansion [19,20]. The Linde-Hampson employs an expansion valve for expansion while the Claude cycle employs an expander [21]. The Linde-Hampson cycle is characterized by a low initial cost and a low efficiency compared with the Claude cycle [22]. Timmer Haus and Flynn [23] suggested

†To whom correspondence should be addressed.
E-mail: seokgoo@kitech.re.kr, kimy3@kw.ac.kr
‡The first authors contributed equally.

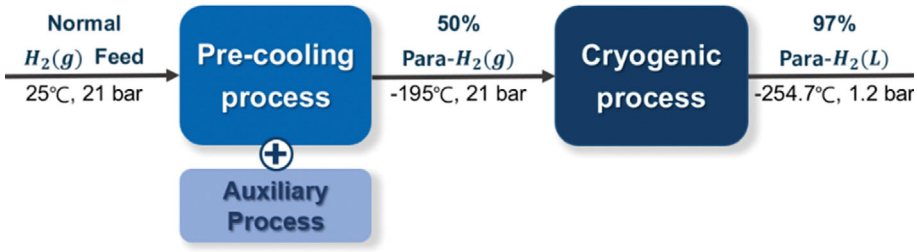

Fig. 1. Conceptual process diagram of the proposed process.

that using the Claude cycle with liquid nitrogen for pre-cooling can improve energy efficiency by approximately 50-70% compared to the Linde-Hampson cycle. The Claude cycle forms the foundation for many other conventional liquefaction processes, as recognized in [24,25].

In the hydrogen liquefaction process, hydrogen is usually pre-cooled from 25 °C to −195 °C and then enters a cryogenic cycle to achieve a final temperature of −253 °C. The newly mixed refrigerant (MR) was investigated for the pre-cooling cycle [26-28]. The MR has a considerably large compressibility and high heat transfer capability, resulting in higher efficiency and lower power consumption for compression. For the cryogenic cycle, various refrigerants such as pure H2 [29] and He [30] are used. Furthermore, in the process proposed by Mirhadi and Medhi [31], two independent MRs are used for pre-cooling and cryogenic cycles, respectively. It leads to considerably higher coefficient of performance compared to other identical processes.

The previous results of energy analysis do not reflect geographical and climatic changes and are limited to specific temperatures (e.g., 25 degrees Celsius). The power consumption of the compressor during the hydrogen cooling process is highly sensitive to the cooling water temperature, which in turn varies according to the season. In general, it can be expected that when the cooling water temperature increases, the power consumption of the compressor increases. This increases the operating energy of the liquefaction process and decreases the exergy efficiency.

In our study, we quantitatively present the results of energy analysis considering the variations in the cooling water temperature. In addition, we suggest a design improvement in the pre-cooling cycle to reduce exergy destruction, where an auxiliary cycle is introduced for the heat exchanger having the greatest exergy destruction. The irreversibility increases as heat exchange progresses for each stream, resulting in the great exergy destruction in the heat exchanger [32]. As the temperature decreases, entropy increases; therefore, it is required to cool the hydrogen stream through multiple stages [33]. Theoretically, exergy destruction is minimized in the reversible situation that reaches the target temperature through an infinite number of cooling steps. However, such a scenario is impractical from economic and engineering points of view [34]. Heat exchangers in the cryogenic cycle show greater exergy destruction than the pre-cooling cycle; however, this is inevitable because the cycle is necessary for reaching the dew point and finally liquefying hydrogen. Since there is a margin to improve the exergy destruction in the pre-cooling cycle, an auxiliary cooling cycle is proposed for the heat exchanger in pre-cooling part. Finally, we evaluate the energy consumption and efficiency of the proposed design.

In Section 2, we propose adding an auxiliary process to the base process and explain its operating condition design. The simulation details are presented in Section 3, and the energy-related terms and the equations are shown in Section 4. The exergy destruction of the proposed design and the investigation of the effects of the cooling water temperature variations are discussed in Section 5.

CONCEPTUAL DESIGN AND PROCESS DESCRIPTION

Fig. 1 shows an overview of the proposed hydrogen liquefaction plant including three steps: the pre-cooling process, the auxiliary cooling process, and the cryogenic process. We used the pre-cooling and cryogenic process design of Mirhadi and Medhi [31] as the base process where the MR compositions are, respectively, optimized for the pre-cooling process and the cryogenic process. We added the auxiliary cooling process to this basic hydrogen liquefaction process.

The process proposed by Mirhadi and Medhi employs the Claude process and the MR in Table 1 as a refrigerant to pre-cool hydrogen from 25 °C to −195 °C. This hydrogen is further sent to a cryogenic cycle to reach a final temperature of −254.7 °C, where Nelium (a mixture of hydrogen, neon, and nitrogen) shown in Table 2 is used as the refrigerant. The feed stream is pure hydro-

Table 1. Refrigerant composition in the pre-cooling process

Material	Mole fraction
Methane	0.17
Ethane	0.07
Propane	0.18
n-Butane	0.02
n-Pentane	0.15
Hydrogen	0.01
Nitrogen	0.16
Refrig-14	0.08
Ethylene	0.16

Table 2. Refrigerant composition in the cryogenic process

Materials	Mole fraction
Neon	0.100
Hydrogen	0.065
Helium	0.835

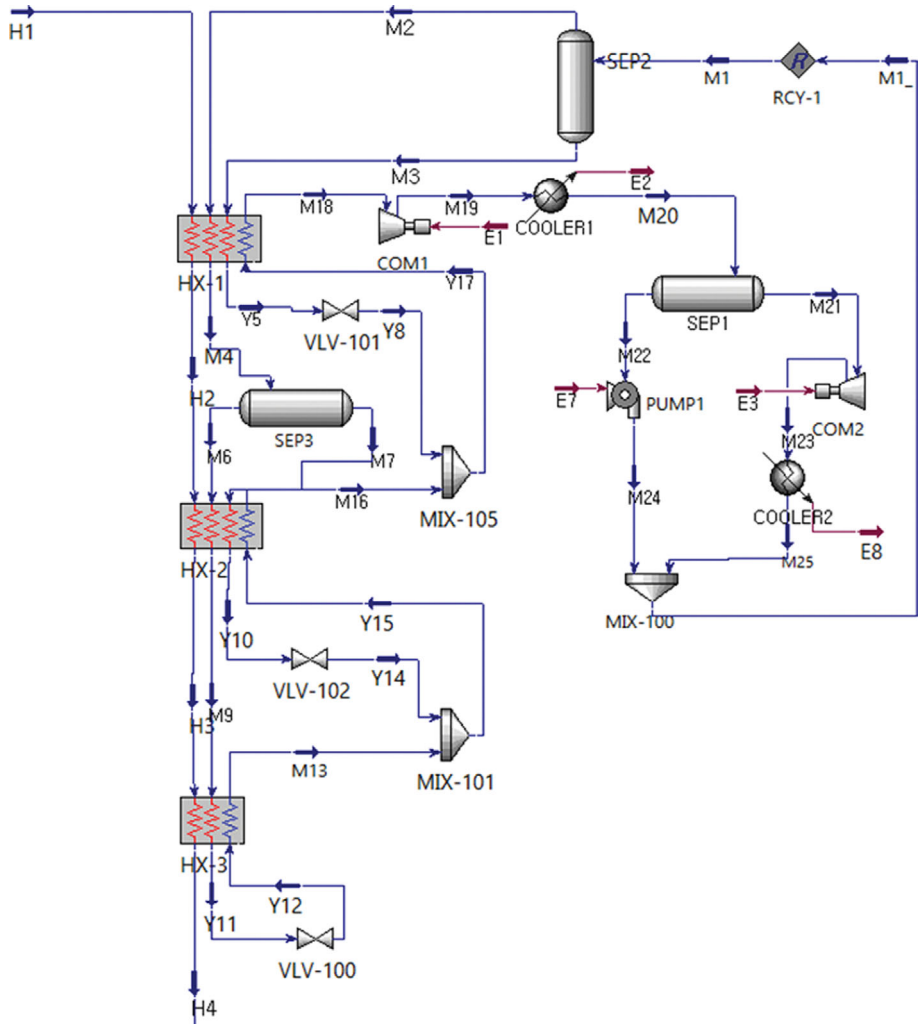

Fig. 2. Flowsheet of the original pre-cooling process for hydrogen liquefaction.

gen at 25 °C and 21 bar, and the flow rate is set as 300 TPD.

The original pre-cooling process, shown in Fig. 2, employs three heat exchangers in pre-cooling: HX-1 (25 °C to –45 °C), HX-2 (–45 °C to −105 °C), and HX-3 (−105 °C to −195 °C). Among the three heat exchangers, we focused on reducing the exergy destruction of HX-3. This is because HX-3 operates in the lowest temperature range in the pre-cooling cycle and contains the largest temperature change. As noted in [31], the amount of exergy destruction of HX-3 is the greatest in the pre-cooling cycle. Therefore, we added another heat exchange cycle between HX-2 and HX-3 to reduce exergy destruction in HX-3. The proposed pre-cooling process with auxiliary process noted as HX-A1 is shown in Fig. 3.

Because our aim was to analyze exergy destruction improvement by the addition of an auxiliary process and the effects of cooling water temperature change, the temperature of the HX-A1 hydrogen inlet was set at −105 °C, which is equal to the temperature of HX-3 hydrogen inlet in the base process. In addition, the temperature of the HX-3 hydrogen outlet was set at −195 °C for the proposed process, which is the same as the base process. In addition, the composition of the mixed refrigerant (MR) used in the pre-cooling and cryogenic cycle is the same as in Mirhadi and Medhi's study [31].

For the auxiliary cycle, hydrogen was adopted as a refrigerant because it is a suitable refrigerant in the temperature range of the auxiliary process (near −105 °C) [29,35]. Regarding the auxiliary cycle, the pressure ratio of the compressor (COM-A1), the flow rate of the refrigerant, and the outlet temperature of HX-A1 main hydrogen stream should be determined. We investigated the case where the outlet temperature of HX-A1 was set as −108 °C, the cooling of 3 °C. The pressure ratio and the refrigerant flow rate in the auxiliary cycle were optimized to maximize the coefficient of performance (COP). Accordingly, the MR flow rate and the pressure ratio in the base pre-cooling cycle were determined. The auxiliary process contributes to reducing the MR flow rate of the main cooling cycle by providing additional cooling. It leads to the reduction of exergy destruction, and it will be discussed in Section 5.

In the cryogenic process shown in Fig. 4, the hydrogen stream is cooled to −254.7 °C through HX-4 to HX-9. During this process, the hydrogen feed is catalytically converted from ortho to para-hydrogen through two converters, respectively. Before HX-4, the ratio of para-hydrogen is adjusted to 50% by CRV-1. After HX-5, the ratio of para-hydrogen reaches about 95% by CRV-2.

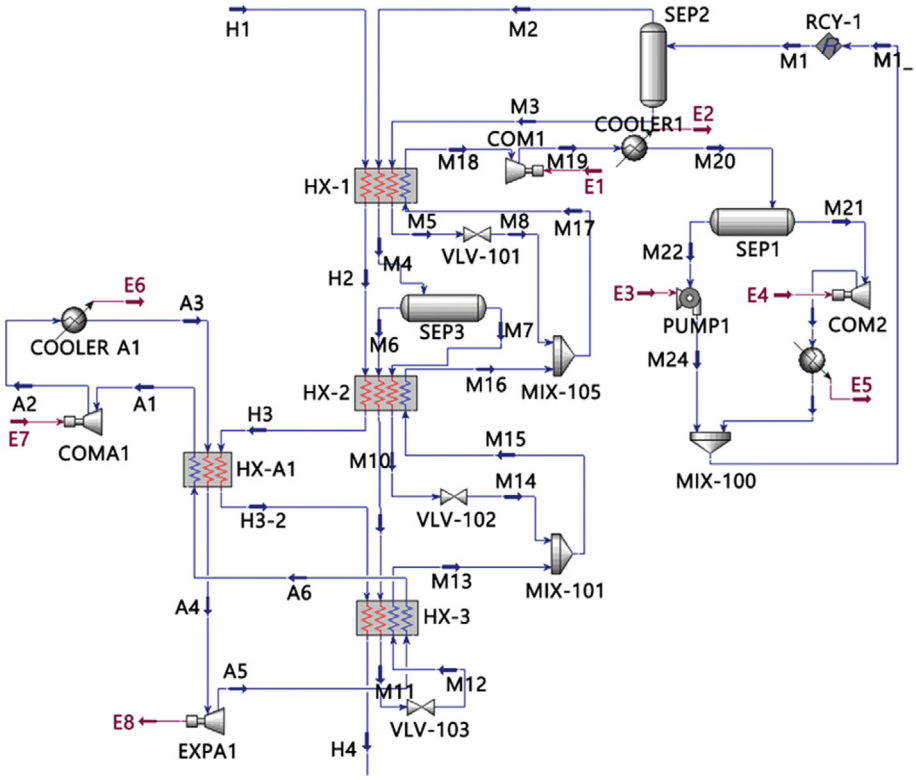

Fig. 3. Flowsheet of the pre-cooling and auxiliary process of the proposed process for hydrogen liquefaction.

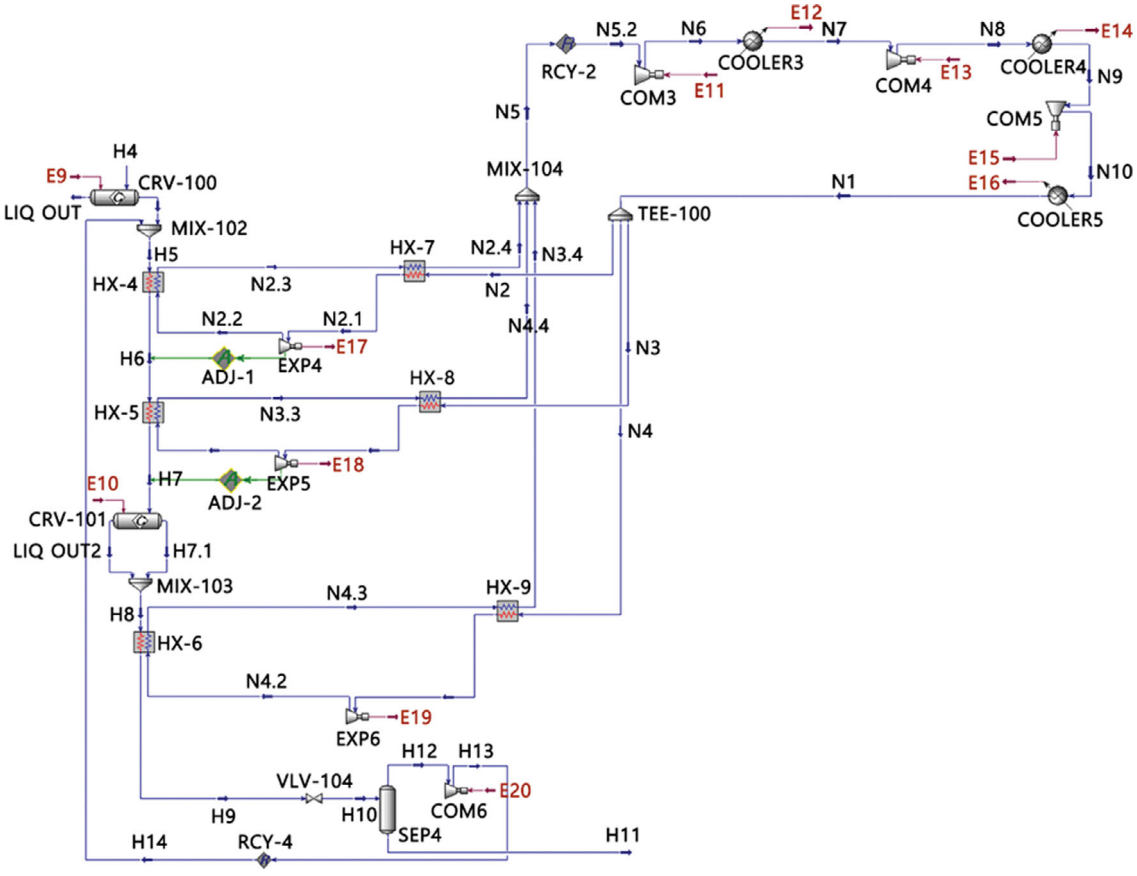

Fig. 4. Flowsheet of the cryogenic process of the proposed process for hydrogen liquefaction.

Table 3. Feed and product streams of the process

Feed condition	25 °C, 21 bar, pure hydrogen
Feed flow rate	300 TPD
Product condition	−254.7 °C, 1.2 bar, 97% para-hydrogen
Product flow rate	12,420 kg/h

Finally, the product has a para-hydrogen fraction of 97% at 1.2 bar and −254.7 °C. When an ortho-para conversion occurs without a catalyst, the reaction speed is very slow and the energy (703.3 kJ/kg) released during the reaction is larger than the latent heat of vaporization (448 kJ/kg) [36], so the produced liquid hydrogen is converted back into gas. Therefore, ortho-para conversion must be performed at an appropriate rate through a catalytic conversion reactor, the simulation details of which are described in Section 3.5. The feed and product streams are summarized in Table 3.

Note that we conducted a simulation in which the ortho-para conversion was considered in two conversion reactors. The conversion reactors were located downstream the modified precooling process. Thus, the conversion heat calculation does not affect the evaluation of the proposed and basic processes or the SEC tendency depending on the cooling water temperature. If the conversion heat is considered continuously with catalytic heat exchangers as discussed in the studies by No et al. [37] and Lee et al. [38], then the SEC could increase more than 20% compared to the one presented in this study.

PROCESS SIMULATION

The process proposed in this study was simulated using Aspen HYSYS, which has a wide range of available data and is excellent for calculating the complex process. The material data mainly came from the HYSYS database. The Peng Robinson-Stryjek-Vera (PRSV) equation considering interaction parameters was used as the thermodynamic equation of state, because this equation is suitable for calculation in a wide range of temperatures and pressure [39,40]. The equation of state applies to various parts of the equipment such as compressors and expanders and it is important for the temperature, pressure, and volume calculations. Since this study does not focus on the analysis of dynamic characteristics of rotating equipment, the efficiencies of the compressor and expander are assumed as 90%.

1. Heat Exchangers

Multistream heat exchangers are used in the hydrogen liquefaction process. To operate a heat exchanger stably, it is necessary to precisely maintain a reasonable temperature difference between the streams during the cooling process [41]. The heat balance between the cold and hot streams in the heat exchanger is described by the following equation [42].

$$m_i C_{pi} \times (T_{h,i} - T_{c,i}) = \sum_{j=1}^{n} A_{i,j} U_{i,j} (T_{m,j} - T_{m,i}) \quad (1)$$

where C_p is the specific heat of the stream, A is the area of heat transfer, and U is the total heat transfer coefficient. i and j denote the hot and the cool streams for this case. Table 4 lists the detailed operating conditions of the ten heat exchangers in the proposed liquefaction process. Although the values of minimum approach temperature seem relatively small, it is a practicable level because cryogenic process such as hydrogen liquefaction uses a highly efficient plate or printed-circuit heat exchanger [43].

2. Compressors

The performance of the compressors depends on various factors such as the inlet and outlet temperatures, molecular weight of the inlet, and the inlet and outlet pressures. The brake horsepower (BHP) of the compressor is calculated as follows [44]:

$$\dot{W}_{BHP} = \frac{\dot{q}_{in} \times P_s \left(\frac{Z_\omega}{Z_{in}}\right) \left\{ \frac{CR^{\frac{k-1}{k}} - 1}{\frac{k-1}{k}} \right\}}{229 \times \eta_{is}} \times (1 + \%\text{Mechanical Loss}) \quad (2)$$

where $\dot{q}_{in}$ is the volume flow rate, k is the specific heat ratio, P_s is

Table 4. Detailed operating conditions of the heat exchangers with cooling water of 25 °C (LMTD: Logarithmic mean temperature difference)

	HX-1	HX-2	HX-3	HX-A1	HX-4
LMTD (°C)	2.791	2.696	2.603	1.626	7.057
Heat duty (kW)	22,982	14,211	12,838	3,133.4	1,354
Minimum approach temperature (°C)	1.084	1.823	1.012	1.000	2.200
	HX-5	HX-6	HX-7	HX-8	HX-9
LMTD (°C)	2.244	6.374	2.475	2.253	2.280
Heat duty (kW)	1,620	933.2	5,786	12,828	15,987
Minimum approach temperature (°C)	1.400	1.500	2.200	1.900	1.800

Table 5. Detailed operating conditions of the compressors with cooling water of 25 °C

	Com-1	Com-2	Com-A1	Com-3	Com-4	Com-5
Pressure ratio	3.50	2.67	2.00	2.25	2.20	2.05
Inlet pressure (bar)	1.80	6.30	1.20	1.50	3.37	7.43
Outlet pressure (bar)	6.30	16.8	2.40	3.38	7.43	15.2
Power (kW)	8,111.18	5,578.51	161.32	17,170.5	16,730.6	15,023.1

the suction pressure, Z is the compression factor, CR is the compression ratio, and η_{is} is the entropy efficiency of the compressor. This was calculated in Aspen using Schultz's polytropic method and the compressor specifications in Table 5.

3. Pumps

Pumps, which are used to increase the liquid pressure, require relatively lower power than compressors. Ideally, work done by the pump can be calculated as follows [45]:

$$\dot{W}_{pump}=\frac{(P_{out}-P_{in})\times \dot{q}}{\rho} \tag{3}$$

where ρ is the liquid density, P_{out} and P_{in} are, respectively, the inlet and outlet pressures, and $\dot{q}$ is the volume flow rate. The actual power can be obtained by dividing the ideal power ($\dot{W}_{pump}$) into the isotropic efficiency of the pump, which is defined as:

$$\eta_{pump}=1-\frac{1}{\dot{W}_{pump}} \tag{4}$$

4. Expanders

Expanders are used to lower the refrigerant temperature in the cooling cycle, lower the temperature of the emitted gas, and produce work through volume expansion. They operate more efficiently than expansion valves under a gas stream. The actual output ($\dot{W}_p$) of the expander is expressed as follows:

$$\dot{W}_p=\dot{m}\eta_{is}c_pT_{in}\left\{1-\left(\frac{P_{in}}{P_{out}}\right)^{\frac{1-k}{k}}\right\} \tag{5}$$

where $\dot{m}$ is the molar flow rate, T_{in} is the inlet temperature, and c_p is the constant-pressure specific heat.

5. Ortho-para Conversion Reactors

H2 has two spin isomers (also called nuclear spin isomers). In ortho-hydrogen, the two proton spins point in the same direction, and in para-hydrogen they point in opposite directions. Under thermal equilibrium at room temperature, para-hydrogen and ortho-hydrogen generally coexist at a ratio of approximately 1 : 3 [46]. Because ortho-hydrogen is slightly higher in energy than para-hydrogen, the former spontaneously converts to the latter and reaches nearly 100% conversion at approximately 20 K, where liquefaction takes place [47]. However, this spontaneous conversion releases approximately 670 kJ/kg of energy, which is higher than the hydrogen evaporation latent heat of 452 kJ/kg [36]. This exothermic process causes undesirable boil-off of the liquefied hydrogen.

Table 6. Conversion coefficients and composition of the two reactors

	CRV-100	CRV-101
C_0	82.74	104.0
C_1	−0.4578	−0.4578
C_2	1.158e-003	1.158e-003
Ortho/Para	50%/50% (at −180.4 °C)	5%/95% (at −237.9 °C)

To improve the efficiency of the hydrogen liquefaction process, we used catalytic ortho-para conversion reactors in the process. Their temperature-dependent conversion can be described by

$$\text{Conversion (\%)}=C_0+C_1\cdot T+C_2\cdot T^2 \tag{6}$$

where C_0, C_1 and C_2 are conversion coefficients and T is the temperature of hydrogen (K). The value of C_0, C_1 and C_2 were adjusted to match the calculated ratio of para-hydrogen leaving the reactor to the experimental data (Table 6) [48]. The first one, CRV-100, achieves 50% ortho-para conversion at −180.4 °C, and the second one, CRV-101, can achieve 95% conversion at −237.9 °C.

ENERGY ANALYSIS

1. Coefficient of Performance (COP)

COP represents the efficiency of a heat pump or air conditioning system. It was used to evaluate the performance of heat exchangers in terms of the amount of cold/heat transferred to the target fluid relative to the energy input. A larger COP means more efficient conversion and transmission of cold and heat [49]:

$$COP=\frac{\dot{m}_{feed,\,GH_2}\times(h_{feed,\,GH_2}-h_{product,\,LH_2})}{\dot{W}_{net}} \tag{7}$$

where $\dot{m}_{feed,\,GH_2}$ is mass flow rate of supplied H2 gas, $h_{feed,\,GH_2}$ is

Table 7. Exergy destruction calculation equation of each equipment

Equipment	Exergy destruction rate ($\dot{I}$)	Efficiency
Compressor [50]	$\dot{I}=\dot{E}x_{in}-\dot{E}x_{out}+\dot{W}_{comp}$	$\eta_{comp}=1-\frac{1}{\dot{W}_{comp}}$
Expander [51]	$\dot{I}=\dot{E}x_{in}-\dot{E}x_{out}-\dot{W}_{exd}$	$\eta_{exd}=\frac{\dot{W}_{exd}}{\sum(\dot{m}\cdot e)_{in}-\sum(\dot{m}\cdot e)_{out}}$
Pump [31]	$\dot{I}=\dot{E}x_{in}-\dot{E}x_{out}+\dot{W}_{pump}$	$\eta_{pump}=1-\frac{1}{\dot{W}_{pump}}$
Heat exchanger [42]	$\dot{I}=\sum\dot{E}x_{in}-\sum\dot{E}x_{out}$	$\eta_{hx}=\frac{\sum\dot{E}x_{out}}{\sum\dot{E}x_{in}}$
Valve [52]	$\dot{I}=\dot{E}x_{in}-\dot{E}x_{out}$	$\eta_{valve}=\frac{\sum\dot{E}x_{out}}{\sum\dot{E}x_{in}}$

the enthalpy per unit mass of supplied H2 gas, $h_{product,\,LH_2}$ is the enthalpy per unit mass of produced liquid hydrogen, and $\dot{W}_{net}$ is the total work.

2. Specific Energy Consumption (SEC)

In the current system, SEC describes the amount of energy required to produce 1 kg of liquid hydrogen. It was calculated by dividing the input work by the flow rate of liquefied hydrogen [44]:

$$SEC = \frac{\dot{W}_{net}}{\dot{m}_{product,\,LH_2} \times 3{,}600}\ [KWh] \tag{8}$$

where $\dot{m}_{product,\,LH_2}$ is the mass flow rate of produced liquid hydrogen. Table 9 summarizes the values of $\dot{W}_{net}$ and SEC of this design according to the cooling water temperature. The details will be discussed in Section 5.

3. Exergy Analysis

Exergy is the maximum amount of work that can be done using a given energy input. Analysis based on the second law of thermodynamics can reveal the degree of irreversibility of the process and the amount of useful energy and work. Specifically, exergy analysis shows where most of the irreversible heat transfer occurs and provides quantitative information about the thermodynamic inefficiency of the overall process. The exergy loss during the process depends on the devices, as summarized in Table 7. The exergy efficiency of the entire process is defined as:

$$\eta_{ex} = \frac{\dot{E}x_{product} - \dot{E}x_{feed}}{\dot{W}_{net}} \tag{9}$$

Based on these formulas, the exergy destruction at various cooling water temperatures was calculated and analyzed in the next section.

RESULTS AND DISCUSSION

The previous sections explained the proposed design with an additional heat exchange cycle. In section 5.1, we first compare the exergy destruction of the proposed process with the process without the auxiliary cycle (called the base process) under the cooling water temperature of 25 °C. In section 5.2, the exergy destruction is analyzed at various cooling water temperatures and compared with that of the base process.

1. Exergy Destruction Analysis at 25 °C

Adding an auxiliary cycle in the pre-cooling cycle reduces the irreversibility, especially in the heat exchanger with the largest exergy destruction (HX-3). SEC was also improved by reducing the power consumption of the main cycle.

Table 8 lists exergy destruction calculated for each device with a cooling water temperature of 25 °C. In the base process, exergy destruction at HX-2 and HX-3 was 532.11 kWh and 1,342.68 kWh, respectively. After introducing a new heat exchange cycle between HX-2 and HX-3, the corresponding value was reduced to 307.53 kWh and 679.66 kWh. Adding the exergy destruction of 313.03 kWh at HX-A1, the sum of HX-A1 and HX-3 was 992.69 kWh.

Table 8. Exergy destruction of each equipment at 25 °C

Device	Exergy destruction (kWh)	
	Base process	Proposed process
HX-1	693.97	430.28
HX-2	532.11	307.53
HX-3	1,342.68	679.66
HX-A1	-	313.03
Com-1	806.72	677.96
Com-2	497.85	477.15
Com-A1	-	86.12
Exp-A1	-	94.41
VLV-1	82.05	119.83
VLV-2	108.56	128.60
VLV-3	369.35	350.87
SUM	4,433.29	3,665.44

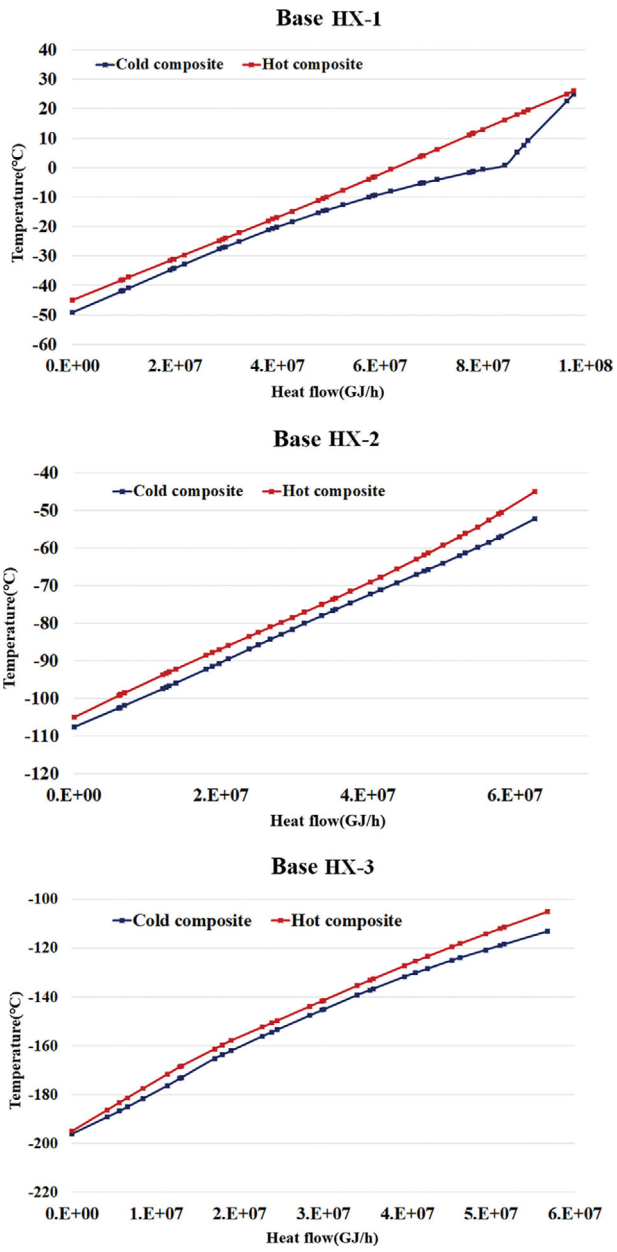

Fig. 5. Composite curve of the heat exchangers HX-1, HX-2, and HX-3 in base process.

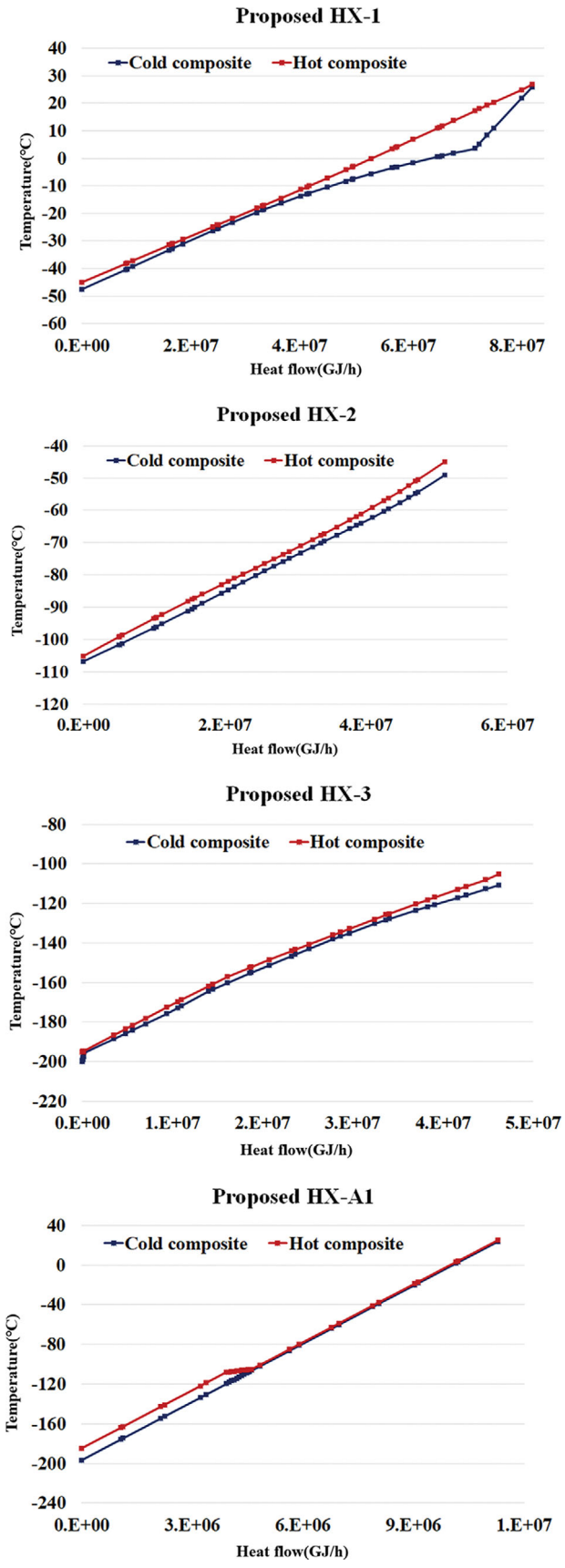

Fig. 6. Composite curve of the heat exchangers HX-1, HX-2, HX-3, and HX-A1 in proposed process.

The overall exergy destruction was reduced from 4,433.29 kWh (base process) to 3,665.44 kWh (proposed process), representing a decline of 767.85 kWh (−17.3%).

In the base process, exergy destruction was the largest at HX-3, and this value was drastically reduced from 1,342.68 to 679.66 kWh by adding an auxiliary process. With the addition of new equipment, total exergy destruction tended to decrease. Fig. 5 shows the temperature-heat flow graph of the pre-cooling cycle in the base process, and Fig. 6 shows the temperature-heat flow graph of the pre-cooling cycle in the proposed process.

The exergy destruction of each equipment in 25 °C of cooling water is shown in Fig. 7. The total exergy destruction of the pre-cooling process of the proposed process is 3,665.44 kWh. In this process, it can be seen that HX-2 has the largest value of 679.46 kW. COM1 and COM2 have the second and third largest values of 677.96 kWh and 477.15 kWh, respectively. COM-A1 has the smallest value of 26.12 kWh.

2. Exergy Analysis Under Cooling Water Temperature Variations

Several coolers are used in the pre-cooling and cryogenic cycle of the proposed process. The temperature of the supplied cooling water is determined by the surrounding environment. In geographical areas with obvious seasonal temperature changes (such as South Korea), the cooling water temperature is expected to fluctuate throughout the year. Hence, we analyzed SEC, exergy destruction, and power consumption at different cooling water temperatures. In this design, the temperature of the cooling water is set to 20, 25, 30, and 35 °C, and the effect of the auxiliary process is investigated in terms of SEC, energy destruction, and power consumption.

In both the base and proposed processes, exergy destruction tends to increase with the cooling water temperature. As the cooling water temperature rises, exergy destruction and power consumption tend to increase. The specific values of exergy destruction and power consumption are listed in Table 9.

The additional auxiliary process reduces exergy destruction at each water temperature The proposed process showed a few improvements as 126.78 kWh at 20 °C. The exergy destruction of the proposed process increased slowly as the cooling water temperature increased, compared with that of the base process, as shown in Fig. 8. Finally, it showed 2,695.04 kWh lower exergy destruction than the base process at 35 °C. Thus, the proposed process had 34.77% lower exergy destruction than that of the base process at 35 °C.

3. SEC and COP Analysis

SEC describes the amount of energy required to produce one unit of product. It is commonly used as a core energy performance indicator. The SEC values are listed in Table 10. At 25 °C, the SEC of the base process was 1.232 and 3.610 kWh/kgLH2 in the pre-cooling and cryogenic steps, respectively. After adding the auxiliary process, these values at the same temperature were 1.173 and 3.610 kWh/kgLH2, respectively. Although the cryogenic process had the same SEC value, it decreased during the pre-cooling process. Thus, adding the auxiliary process lowered the exergy destruction and SEC, making the process more efficient in terms of energy consumption.

The SEC values in both processes increase by increasing cooling water temperature. The rate of increase in SEC is also lower

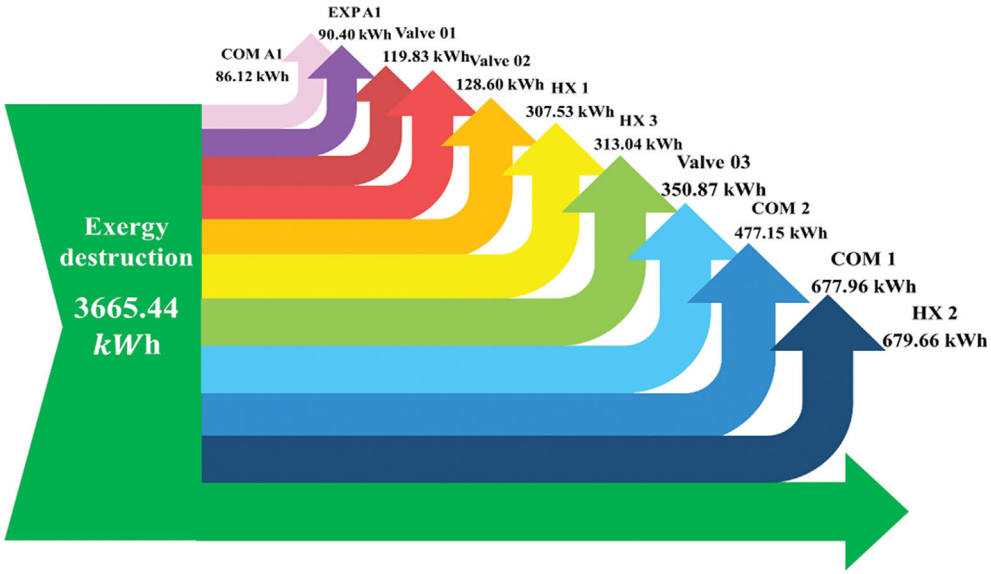

Fig. 7. Exergy destruction analysis of the proposed process in the pre-cooling cycle at 25 °C.

Table 9. Exergy destruction and power consumption of each process

Cooling water temperature	Exergy destruction (kWh)			Power consumption (kW)		
	Base process	Proposed process	Percent change (%)	Base process	Proposed process	Percent change (%)
20 °C	3,701.63	3,574.85	−3.42	58,055.09	58,009.71	−0.08
25 °C	4,433.30	3,665.45	−17.32	60,139.06	59,404.17	−1.22
30 °C	5,689.58	4,350.65	−23.53	62,884.79	61,478.96	−2.23
35 °C	7,750.91	5,055.87	−34.77	66,553.76	63,631.04	−4.39

Table 10. Percent changes in SEC at different cooling water temperatures

Cooling water temperature	SEC (kWh/kgLH2)			COP		
	Base process	Proposed process	Percent change (%)	Base process	Proposed process	Percent change (%)
20 °C	4.674	4.670	−0.09	0.2530	0.2533	+0.12
25 °C	4.842	4.783	−1.22	0.2443	0.2473	+1.62
30 °C	5.063	4.950	−2.23	0.2346	0.2389	+1.80
35 °C	5.359	5.123	−4.40	0.2208	0.2309	+4.37

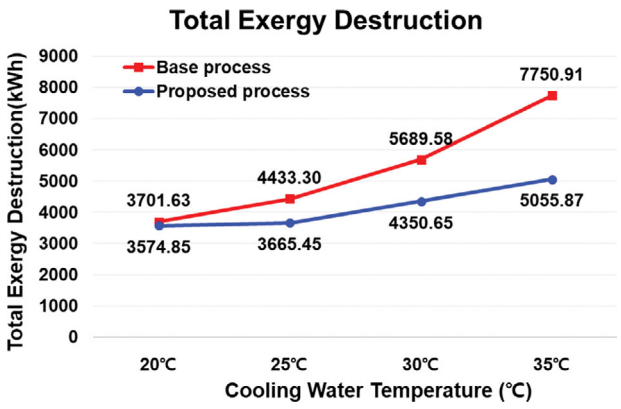

Fig. 8. Total exergy destruction of the pre-cooling cycle.

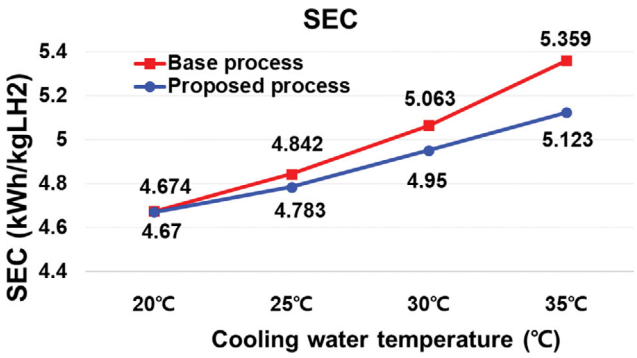

Fig. 9. SEC changes according to the cooling water temperature.

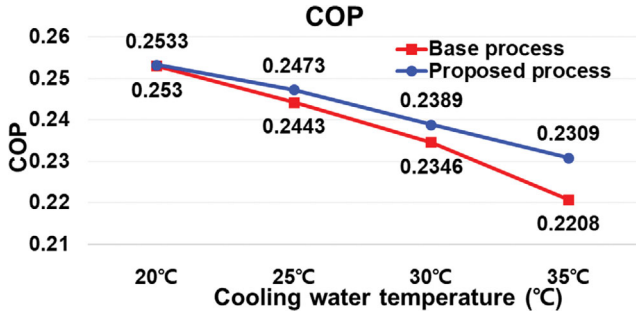

Fig. 10. COP change according to the cooling water temperature.

with the auxiliary process than with the base process. Therefore, the additional auxiliary process lessens exergy destruction much at higher ambient temperatures as shown in Fig. 9.

The COP values are listed in Table 10. COP of both processes decreased by increasing of cooling water temperature, as shown in Fig. 10. The proposed process showed a few improvements in the range of 20 °C, but it decreased slowly as the cooling water temperature increased. As a result, the proposed process showed much higher COP than that of the base process as the temperature increased.

CONCLUSIONS AND FUTURE WORKS

The effects of variation in cooling water temperature on the hydrogen liquefaction process were quantitatively analyzed by investigating exergy destruction, SEC, and COP. In addition, an auxiliary cooling cycle was proposed for the heat exchanger with the highest exergy destruction in the pre-cooling section. As the cooling water temperature increased, the SEC increased, and the COP decreased due to the reduced heat dissipation to the environment. The proposed auxiliary cycle reduced the increase rate of SEC and the decrease rate of COP compared to the base process without the auxiliary cycle. This was achieved by the lower total exergy destruction with the proposed process compared to the base case. In particular, at 35 °C, the exergy destruction of the proposed process was reduced by 34.77% than the base case. These results show that the efficient cooling provided by the auxiliary cycle can enhance the robustness of the process to variations in ambient temperatures.

In Elizabeth et al., the DOE Hydrogen and Fuel Cells Program Record [53], the capital cost contribution to the liquefaction process decreases as production capacity increases. Future work could include further optimization of operating conditions using genetic algorithm [54] and a comprehensive economic analysis of additional equipment costs. In addition, the conversion heat will be considered continuously in catalytic heat exchangers, using the equilibrium hydrogen heat capacity as studied by No et al. [37] and Lee et al. [38].

ACKNOWLEDGEMENTS

This work is supported by the Korea Institute of Energy Technology Evaluation and Planning (KETEP), granted financial resources from the Ministry of Trade, Industry, and Energy (No. 20227310100010) and by the Korea Agency for Infrastructure Technology Advancement (KAIA) grant funded by the Ministry of Land, Infrastructure and Transport (No. 21ATOG-C162087-01).

NOMENCLATURE

A : heat transfer area
C_p : specific heat capacity [kJ/kmole °C]
CR : compression ratio
Ex : rate of exergy [kW]
I : irreversibility [kW]
k : specific heat ratio
LMTD : logarithmic mean temperature difference
ρ : liquid density [kg/m^3]
$\dot{m}$: molar flow rate [kmole/s]
P : pressure [bar]
q : volumetric flow rate [m^3/h]
T : temperature
U : overall heat transfer coefficient [kW/m^3·°C]
$\dot{W}$: work transfer rate [kW]
x : component mole fraction
Z : gas compressibility factor

Greek Letters

η : efficiency

Abbreviation

SEC : specific energy consumption
COM : compressor
COP : coefficient of performance
EXP : expander
CRV : conversion reactor
HX : heat exchanger

Subscripts

BHP : brake horsepower
c : cold
Ex : exergy
H : hot
i : component i
o : outlet
P : pump
s : suction

Superscripts

° : standard condition

REFERENCES

1. R. P. Date, N. O. Asia and M. East, Global and regional coal phase out requirements of the paris agreement: Insights from the IPCC special report on 1.5 C (2019).
2. F. Wu, N. Huang, F. Zhang, L. Niu and Y. Zhang, *Technol. Forecast Soc. Change*, **159**, 120198 (2020).
3. A. Kuriyama, K. Tamura and T. Kuramochi, *Energy Policy*, **130**, 328 (2019).

4. R. Karacan, S. Mukhtarov, İ. Barış, A. İşleyen and M. E. Yardımcı, *Energies*, **14**(10), 2947 (2021).
5. S. D. Oladipupo, H. Rjoub, D. Kirikkaleli and T. S. Adebayo, *Int. J. Renew. Energy Dev.,* **11**(1) (2022).
6. P. P. Edwards, V. L. Kuznetsov and W. I. David, *Philos. Trans. Royal Soc. A*, **365**(1853), 1043 (2007).
7. A. Midilli, M. Ay, I. Dincer and M. A. Rosen, *Renew. Sust. Energ. Rev.*, **9**(3), 255 (2005).
8. T. N. Veziroğlu and S. Şahi, *Energy Convers. Manag.*, **49**(7), 1820 (2008).
9. K. Cheon and J. Kim, *J. Korean Soc. Miner. Energy Resour. Eng.*, **57**(6), 629 (2020).
10. S. K. Kar, A. S. K. Sinha, R. Bansal, B. Shabani and S. Harichandan, *WIREs Energy Environ.*, **12**(1), e457 (2022).
11. C. Philibert, Perspectives on a hydrogen strategy for the european union, *Etudes de l'Ifri, Ifri.*, **51**(28), 49 (2020).
12. B. H. Park and D. H. Lee, *Korean J. Chem. Eng.*, **39**(4), 902 (2022).
13. A. Züttel, *Naturwissenschaften*, **91**(4), 157 (2004).
14. A. Züttel, *Mater. Today*, **6**(9), 24 (2003).
15. U. Eberle, M. Felderhoff and F. Schueth, *Angew. Chem., Int. Ed.*, **48**(36), 6608 (2009).
16. S. Krasae-in, J. H. Stang and P. Neksa, *Int. J. Hydrogen Energy*, **35**(10), 4524 (2010).
17. J. Andersson and S. Grönkvist, *Int. J. Hydrogen Energy*, **44**(23), 11901 (2019).
18. S. Y. Kim and D. K. Choi, *Korean Ind. Chem. News*, **21**(3), 20 (2018).
19. U. Cardella, L. Decker, J. Sundberg and H. Klein, *Int. J. Hydrogen Energy*, **42**(17), 12339 (2017).
20. S. Bischoff and L. Decker, *AIP Conference Proc.*, **1218**(1), 887 (2010).
21. A. Tarique, I. Dincer and C. Zamfirescu, Application of scroll expander in cryogenic process of hydrogen liquefaction, In: *Progress in exergy, energy, and the environment*, Springer, 91 (2014).
22. R. F. Abdo, H. T. Pedro, R. N. Koury, L. Machado, C. F. Coimbra and M. P. Porto, *Energy*, **90**, 1024 (2015).
23. K. D. Timmerhaus and T. M. Flynn, *Cryogenic process engineering*, Springer Science & Business Media (2013).
24. T. K. Nandi and S. Sarangi, *Int. J. Hydrogen Energy*, **18**(2), 131 (1993).
25. D. Berstad, G. Skaugen and Ø. Wilhelmsen, *Int. J. Hydrogen Energy*, **46**(11), 8014 (2021).
26. C. W. Park, K. S. Cha, S. G. Lee, C. G. Lee and K. H. Choi, *J. Kor. Inst. Gas.*, **17**(1), 67 (2013).
27. S. Krasae-In, J. H. Stang and P. Neksa, *Int. J. Hydrogen Energy*, **35**(22), 12531 (2010).
28. S. Krasae-In, A. M. Bredesen, J. H. Stang and P. Neksa, *Int. J. Hydrogen Energy*, **36**(1), 907 (2011).
29. S. Krasae-In, *Int. J. Hydrogen Energy*, **39**(13), 7015 (2014).
30. G. Valenti and E. Macchi, *Int. J. Hydrogen Energy*, **33**(12), 3116 (2008).
31. M. S. Sadaghiani and M. Mehrpooya, *Int. J. Hydrogen Energy*, **42**(9), 6033 (2017).
32. M. Mehdizadeh-Fard, F. Pourfayaz and A. Maleki, *Energy Rep.*, 7, 174 (2021).
33. H. Zhang, J. Baeyens, G. Caceres, J. Degreve and Y. Lv, *Prog. Energy Combust. Sci.*, **53**, 1 (2016).
34. H. Ansarinasab, M. Mehrpooya and A. Mohammadi, *J. Clean Prod.*, **144**, 248 (2017).
35. M. Mehrpooya, M. S. Sadaghiani and N. Hedayat, *Int. J. Energy Res.*, **44**(3), 1636 (2020).
36. M. Asadnia and M. Mehrpooya, *Int. J. Hydrogen Energy*, **42**(23), 15564 (2017).
37. W. Noh, S. Park, J. Kim and I. Lee, *Int. J. Energy Res.*, **46**(9), 12926 (2022).
38. D. Lee, D. Q. Gbadago, Y. Jo, G. Hwang, Y. Jo, R. Smith and S. Hwang, *Energy Convers. Manag.*, **245**, 114620 (2021).
39. D. Peng and D. B. Robinson, *Ind. Eng. Chem.*, **15**(1), 59 (1976).
40. R. D. McCarty, J. Hord and H. M. Roder, *Selected properties of hydrogen (engineering design data),* US Department of Commerce, National Bureau of Standards (1981).
41. M. Mehrpooya, M. M. M. Sharifzadeh and M. A. Rosen, *Energy*, **90**, 2047 (2015).
42. M. Picon-Nunez, G. T. Polley and M. Medina-Flores, *Appl. Therm. Eng.*, **22**(14), 1643 (2002).
43. A. Naquash, M. A. Qyyum, S. Min, S. Lee and M. Lee, *Energy Convers. Manag.*, **251**, 114947 (2022).
44. A. Giampaolo, *Compressor handbook: Principles and practice*, CRC Press (2020).
45. S. M. Yahya, *Turbines compressors and fans*, Tata McGraw-Hill Education (2010).
46. E. Ilisca, *Prog. Surf. Sci.*, **41**(3), 217 (1992).
47. S. Gursu, M. Lordgooei, S. A. Sherif and T. N. Veziroğlu, *Int. J. Hydrogen Energy*, **17**(3), 227 (1992).
48. A. Riaz, M. A. Qyyum, A. Hussain and M. Lee, *Int. J. Hydrogen Energy*, In Press (2022).
49. I. Dincer and M. A. Rosen, *Thermal energy storage: Systems and applications,* John Wiley & Sons (2021).
50. I. J. Karassik, J. P. Messina, P. Cooper and C. C. Heald, *Pump handbook*, McGraw-Hill Education (2008).
51. H. Mahabadipour and H. Ghaebi, *Appl. Therm. Eng.*, **50**(1), 771 (2013).
52. M. Kanoğlu, *Int. J. Energy Res.*, **26**(8), 763 (2002).
53. E. Connelly, M. Penev, A. Elgowainy and C. Hunter, Current status of hydrogen liquefaction costs, *DOE Hydrogen and Fuel Cells Program Record.*, 1-10 (2019).
54. M. Jeong, E. Cho, H. Byun and C. Kang, *Korean J. Chem. Eng.*, **38**, 380 (2021).